Association and Joint Optimization of max-dmin Precoder with MIMO Turbo Equalization

Nhat Quang Nhan, Philippe Rostaing, Karine Amis Cavalec, Ludovic Collin, Emanuel Radoi

Association and Joint Optimization of max-$d_{\min}$ Precoder with MIMO Turbo Equalization

Nhat-Quang Nhan*†, Philippe Rostaing*, Karine Amis†, Ludovic Collin*, and Emanuel Radoi*
* Université Européenne de Bretagne; Université de Brest; CNRS, UMR 6285 Lab-STICC, France,
Email: {nhat-quang.nhan, philippe.rostaing, ludovic.collin, emanuel.radoi}@univ-brest.fr
† Institut Mines-Telecom; Telecom Bretagne; Signal and Communications department;
CNRS, UMR 6285 Lab-STICC, Technopôle Brest-Iroise CS 83818, 29238 Brest Cedex 3, France,

Abstract—In this paper, we investigate the concatenation of the multiple input multiple output (MIMO) max-$d_{\min}$ linear precoder with an outer forward error correction (FEC) code at the transmitter. At the receiver side, the turbo equalization is taken into account, which iteratively exchanges the *extrinsic* information between a minimum mean square error interference canceller (MMSE IC) and a FEC decoder. The analysis done by extrinsic information transfer (EXIT) chart shows that a higher mutual information (MI) at the convergence state of the turbo equalization is observed thanks to the linear precoder. In addi-tion, we exploit this property to propose a new precoder named max-$d_{\min}$-mod. Numerical simulations are in accordance with the theoretical analysis, which exhibits a significant improvement of the error-rate of the turbo equalization as well as a significant gain of max-$d_{\min}$-mod compared to original max-$d_{\min}$ precoder.

Keywords—Linear precoder, turbo equalization, iterative receiver.

I. Introduction

Invented by C. Berrou [1], the turbo principle has become essential to take up the challenge of near Shannon limit in communication systems. One of its well-known applications is turbo equalization, which was introduced the first time in [2] and later improved in [3], [4]. The modern turbo equalization takes into account the iterative information exchanges not only between the MMSE IC and the FEC decoder, but also between the FEC decoder and the symbol-to-binary converter. Recent researches show that, by applying the intersymbol interference cancellation criterion, the turbo equalization significantly improves the system performance [5], [6].

On the other hand, the advantages of using multiple antennas at transmitter and receiver of a wireless multiple-input multiple-output (MIMO) system has been well exploited in the recent years [7]. By using multiple antenna transceivers, MIMO technology not only offers multiplexing and diversity gains, but it also achieves higher conventional point-to-point link reliability in comparison with single transceiver systems [8]. The main challenge is to design a MIMO scheme that fully exploits the presence of multiple antennas. In fact, in [9]–[11], multiple copies of transmitted data symbols have been proposed to map across antennas for diversity and transmission robustness. The association of this technique with iterative receivers has shown promising performance [12], [13]. More importantly, in time domain duplex (TDD) closed-loop schemes, the channel state information (CSI) is readily available at the transmitter through a feedback link, which allows us to further design a precoder that is able to adapt to the channel conditions. Indeed, several kinds of linear precoders have been proposed in the literature. They are designed according to different criteria such as maximization of the minimum Euclidean distance in the received constellation (referred to as $\max$-$d_{\min}$ [14]), minimization of bit-error-rate (BER) [15] or maximization of mutual information [16]. However, the outer FEC code is not taken into account in most of the recent designs of linear precoder [17]. In the case of two data streams transmission, $\max$-$d_{\min}$ shows a good uncoded error-rate performance with maximum likelihood detection compared to the listed precoders. In this case, the $\max$-$d_{\min}$ precoder consists of two sub-precoders and switches between them according to the channel angle, which is defined by a ratio between singular values of the channel matrix. The switching threshold has been selected so as to maximize the minimum Euclidean distance in the received constellation of the uncoded system.

In this paper, we propose an association and joint optimization of the $\max$-$d_{\min}$ MIMO linear precoder in the turbo equalization scheme. Our main contributions are threefold. First, we introduce a novel study case that takes into account the concatenation of the MIMO precoder with an outer FEC code assuming a turbo equalization at the receiver. Second, we prove that the MIMO precoder, which usefully maximizes the *extrinsic* MI at the convergence state of the iterative system, plays an essential role in error-rate performance of the turbo equalization. Third, we propose a new $\max$-$d_{\min}$-mod precoder, which aims to optimize the switching threshold of the $\max$-$d_{\min}$ precoder under the constraint of maximizing the *extrinsic* MI at the convergence state. Simulation results show that, there is significant improvement of the error-rate performance of the turbo equalization thanks to the $\max$-$d_{\min}$ precoder. In addition, by using the new $\max$-$d_{\min}$-mod precoder, performance of the iterative system is even more significantly improved.

The remainder of this paper is organized as follows. Section II briefly introduces the system model along with the $\max$-$d_{\min}$ MIMO precoder. Main expressions of the low-complexity interference canceller, which takes into account the associated MIMO precoder, are also presented. In Section III, the role of the MIMO linear precoder in the turbo

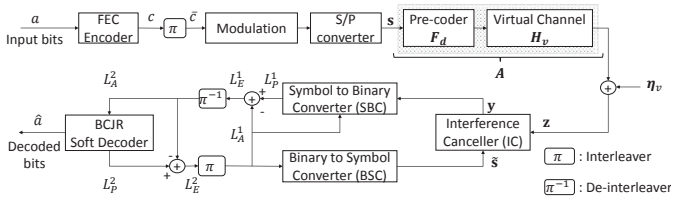

Fig. 1: Equivalent system model.

equalization systems is discussed from EXIT charts. The new max-$d_{\min}$-mod precoder is proposed in this section as well. Simulated error rates are presented in Section IV to validate the theoretical analysis. Section V concludes the paper and gives some perspectives.

II. System model and preliminaries

A. System model

Let us consider a MIMO system with n_R receive, n_T transmit antennas and b independent data streams to be transmitted. We assume that both the transmitter and the receiver have the full-CSI. A binary recursive-systematic convolutional (RSC) code is used to encode the information binary sequence. The FEC codeword is interleaved before being mapped onto quaternary quadrature amplitude modulation (4-QAM) symbols. The mapped symbols are converted into a b-dimensional symbol vector $\mathbf{s}$. The vector $\mathbf{s}$ is then precoded by a precoder $\mathbf{F}$ and transmitted through the MIMO channel. At the receiver, after MIMO detection, an interference canceller iteratively exchanges *extrinsic* information with a BCJR soft decoder [18] by using the soft symbol-to-binary (SBC) and binary-to-symbol converter (BSC). The received vector, denoted by $\mathbf{z}$, reads

$$\mathbf{z} = \mathbf{GHFs} + \mathbf{G}\boldsymbol{\eta}, \tag{1}$$

where $\mathbf{F}$ is the $n_T \times b$ precoding matrix with the power constraint $\|\mathbf{F}\|_F^2 = 1$, $\mathbf{G}$ is the $b \times n_R$ detection matrix, $\mathbf{H}$ is the $n_R \times n_T$ channel matrix, and $\boldsymbol{\eta}$ is the $n_R \times 1$ additive white circularly-symmetric complex gaussian noise vector. We assume $\mathrm{E}[\boldsymbol{\eta}\boldsymbol{\eta}^\dagger] = \sigma_\eta^2 \mathbf{I}_{n_R}$ and $\mathrm{E}[\mathbf{ss}^\dagger] = \sigma_s^2 \mathbf{I}_b$, where $\mathrm{E}[.]$ and $(.)^\dagger$ stand for the mathematical expectation and the conjugate transpose respectively. The $\mathbf{I}_{n_R}$ is an identity matrix of size n_R.

In this paper, we apply the same channel transformation as in [14]. Let us define $\mathbf{F}_d$ and $\mathbf{F}_v$ such that $\mathbf{F} = \mathbf{F}_v \times \mathbf{F}_d$. Matrices $\mathbf{F}_v$ and $\mathbf{G}$ are unitary and chosen so as to transform the MIMO channel into a virtual channel with b independent parallel sub-channels, *i.e.* the columns of $\mathbf{F}_v$ and $\mathbf{G}^\dagger$ respectively are the b most significant right-singular and left-singular vectors of the singular value decomposition of $\mathbf{H}$. Note that $\mathbf{F}_d$ denotes the new precoding matrix. It also satisfies the power constraint $\|\mathbf{F}_d\|_F^2 = 1$. The equivalent model is written as

$$\mathbf{z} = \mathbf{H}_v \mathbf{F}_d \mathbf{s} + \boldsymbol{\eta}_v, \tag{2}$$

where $\boldsymbol{\eta}_v$ is the $b \times 1$ virtual noise vector with $\mathrm{E}[\boldsymbol{\eta}_v \boldsymbol{\eta}_v^\dagger] = \sigma_\eta^2 \mathbf{I}_b$. The matrix $\mathbf{H}_v = \mathrm{diag}(\sigma_1, ..., \sigma_b)$ is the $b \times b$ eigen-channel matrix, where $\{\sigma_1, ..., \sigma_b\}$ are the b most significant singular values of $\mathbf{H}$ sorted in descending order.

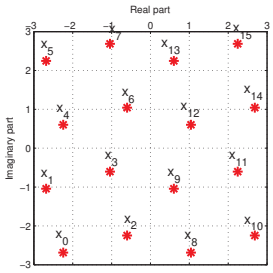

Fig. 2: Received constellation $\mathbf{x}_i$ on the first sub-channel in case $\mathbf{F}_d = \mathbf{F}_{r_1}$.

The equivalent system scheme is shown in Fig. 1, where L_A^1, L_P^1 and L_E^1 respectively stand for the *a priori*, the *a posteriori* and the *extrinsic* log likelihood ratios (LLRs) of the SBC, while the equivalent notations for the BCJR soft decoder are L_A^2, L_P^2 and L_E^2.

B. The max-$d_{\min}$ linear precoder

We focus on a commonly used precoder named max-$d_{\min}$ [14], in which, $\mathbf{F}_d$ was designed to maximize the minimum Euclidean distance, denoted by $d_{min} = \min_{m \neq \ell} \|\mathbf{x}_m - \mathbf{x}_\ell\|$ where $\mathbf{x} = \mathbf{H}_v \mathbf{F}_d \mathbf{s}$, between the received constellation symbols. We restrict ourselves to $b = 2$. The conversion from cartesian to polar form of $\mathbf{H}_v$ gives

$$\mathbf{H}_v = \begin{pmatrix} \sigma_1 & 0 \\ 0 & \sigma_2 \end{pmatrix} = \rho \begin{pmatrix} \cos\gamma & 0 \\ 0 & \sin\gamma \end{pmatrix}, \tag{3}$$

where ρ and γ respectively represent the channel gain and angle. As $\sigma_1 \geq \sigma_2 > 0$, we have $0 < \gamma \leq \pi/4$. Hence, the optimal solution depends on γ and by defining the threshold $\gamma_0 = \arctan\sqrt{\frac{\sqrt{2}-1}{2\sqrt{2}+\sqrt{6}-1}}$ ($\approx 17,28^0$), $\mathbf{F}_d$ reads

- if $0 \leq \gamma \leq \gamma_0$

$$\mathbf{F}_d = \mathbf{F}_{r_1} = \begin{pmatrix} \sqrt{\frac{3+\sqrt{3}}{6}} & \sqrt{\frac{3-\sqrt{3}}{6}} e^{i\frac{\pi}{12}} \\ 0 & 0 \end{pmatrix}, \tag{4}$$

- if $\gamma_0 < \gamma \leq \pi/4$

$$\mathbf{F}_d = \mathbf{F}_{octa} = \frac{1}{\sqrt{2}} \begin{pmatrix} \cos\psi & 0 \\ 0 & \sin\psi \end{pmatrix} \begin{pmatrix} 1 & e^{i\frac{\pi}{4}} \\ -1 & e^{i\frac{\pi}{4}} \end{pmatrix}, \tag{5}$$

where $\psi = \arctan\frac{\sqrt{2}-1}{\tan\gamma}$.

In the case $\gamma \leq \gamma_0$, *i.e.* $\mathbf{F}_d = \mathbf{F}_{r_1}$, the precoder only spreads power on the first sub-channel. Fig. 2 shows the received constellation on the first sub-channel of precoder max-$d_{\min}$ in this case. The constellation is similar to the one of 16-QAM modulation with a rotation by 15^o in each quadrant. On the other hand, in the case $\gamma > \gamma_0$, *i.e.* $\mathbf{F}_d = \mathbf{F}_{octa}$, the precoder spreads power on both sub-channels, where the received constellations are shown in Fig. 3. It is shown that, thanks to the optimization criterion, a pair of neighbor symbols in the first sub-channel, *e.g.* $\mathbf{x}_3$ and $\mathbf{x}_4$, is separated in the second sub-channel.

Fig 4 shows the received $d_{\min}$ normalized by ρ of $\mathbf{F}_{r1}$ and $\mathbf{F}_{octa}$. We can see that, in order to keep the high value of the received normalized $d_{\min}$, the max-$d_{\min}$ precoder uses γ_0 as a threshold to switch between $\mathbf{F}_{r1}$ and $\mathbf{F}_{octa}$. Note that γ_0

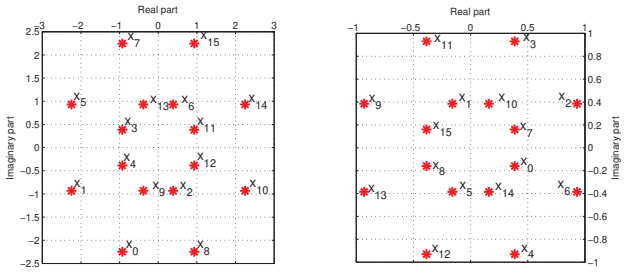

(a) First sub-channel. (b) Second sub-channel.

Fig. 3: Received constellation $\mathbf{x}_i$ on the first and second sub-channels in case $\mathbf{F}_d = \mathbf{F}_{octa}$.

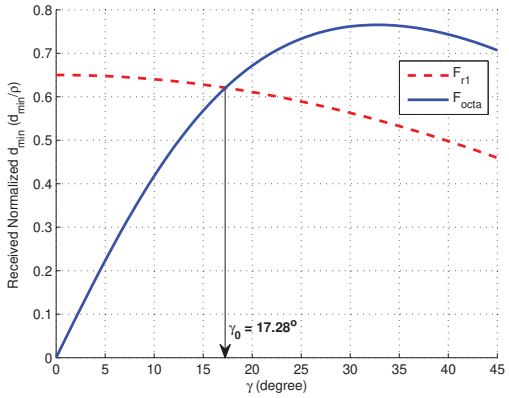

Fig. 4: The received normalized $d_{\min}$ versus γ.

is signal-to-noise ratio (SNR)-independent and designed for uncoded system. The study of this threshold for the coded system under assumption of turbo equalization at the receiver will be presented in Section III-B.

C. Precoded Interference Canceller

In this subsection, we briefly derive the MMSE IC block of the turbo equalization, while taking into account the presence of precoder $\mathbf{F}_d$ at the transmitter side. For further information on turbo equalization, the reader can refer to [19], [20].

The IC consists of a feed-forward and a feedback filter, which are respectively denoted by $\mathbf{W}$ and $\mathbf{Q}$. Both filters are matrices of size $b \times b$. At the output of the IC, the detected vector $\mathbf{y}$ reads

$$\mathbf{y} = \mathbf{W}\mathbf{z} - \mathbf{Q}\tilde{\mathbf{s}}, \tag{6}$$

where $\tilde{\mathbf{s}}$, which is obtained from the output of the BSC (see Fig. 1), is the estimation of symbol vector $\mathbf{s}$ and we assume $\mathrm{E}[\tilde{\mathbf{s}}\tilde{\mathbf{s}}^\dagger] = \sigma_{\tilde{s}}^2\mathbf{I}_b$. The filters $\mathbf{W}$, $\mathbf{Q}$ are obtained from MMSE criterion. The optimization problem can be written as [6]

$$\begin{cases} \min\limits_{\mathbf{W},\mathbf{Q}} \mathrm{E}\big[\|\mathbf{y}-\mathbf{s}\|^2\big], \\ \text{subject to} \quad \mathbf{Q}_{ii} = 0 \quad \forall i, \end{cases} \tag{7}$$

where the constraint means that only the inter-symbol interference has to be canceled.

Let us define $\mathbf{A} = \mathbf{H}_v\mathbf{F}_d$ and $\mathbf{B} = (\sigma_s^2 - \sigma_{\tilde{s}}^2)\mathbf{A}\mathbf{A}^\dagger + \sigma_\eta^2\mathbf{I}_b$. Using the Lagrangian multipliers, the optimization problem yields

$$\mathbf{W}_{k,:} = \sigma_s^2\mathbf{A}_{:,k}^\dagger\big(\mathbf{B} + \sigma_{\tilde{s}}^2\mathbf{A}_{:,k}\mathbf{A}_{:,k}^\dagger\big)^{-1}, \tag{8}$$

and

$$\mathbf{Q}_{k,:} = \mathbf{W}_{k,:}\mathbf{A} - \mathbf{W}_{k,:}\mathbf{A}_{:,k}e_k, \tag{9}$$

where e_k is the k^{th} row of $\mathbf{I}_b$ and the dagger notation ($\mathbf{A}^\dagger$) denotes the conjugate transpose of matrix $\mathbf{A}$. $\mathbf{A}_{:,k}$ and $\mathbf{A}_{k,:}$ respectively denote the k^{th} column and k^{th} row of $\mathbf{A}$.

Let us define $\big(\mathbf{B} + \sigma_{\tilde{s}}^2\mathbf{A}_{:,k}\mathbf{A}_{:,k}^\dagger\big)^{-1} = \mathbf{C}$. Then, the computation cost of $\mathbf{W}_{k,:}$ can be reduced by using the Woodbury's theorem, which yields

$$\mathbf{C} = \mathbf{B}^{-1} - \frac{\sigma_{\tilde{s}}^2}{1 + \sigma_{\tilde{s}}^2\mathbf{A}_{:,k}^\dagger\mathbf{B}^{-1}\mathbf{A}_{:,k}}\mathbf{B}^{-1}\mathbf{A}_{:,k}\mathbf{A}_{:,k}^\dagger\mathbf{B}^{-1}. \tag{10}$$

Hence, we can also deduce the following expression

$$0 < \mathbf{W}_{k,:}\mathbf{A}_{:,k} = \frac{\sigma_{\tilde{s}}^2\mathbf{A}_{:,k}^\dagger\mathbf{B}^{-1}\mathbf{A}_{:,k}}{1 + \sigma_{\tilde{s}}^2\mathbf{A}_{:,k}^\dagger\mathbf{B}^{-1}\mathbf{A}_{:,k}} = \mu_k < 1. \tag{11}$$

Finally, the IC output can be modeled as follows

$$y_k = \mu_k s_k + \xi_k \quad \text{for } k \in \{1,\ldots,b\}, \tag{12}$$

where ξ_k is independent from s_k, has gaussian distribution with zero mean and variance $\sigma_{\xi_k}^2 = \sigma_s^2\mu_k(1-\mu_k)$. Thus, the signal-to-noise ratio at IC output is denoted by $p_k = \frac{\mu_k}{1-\mu_k}$.

Let $\mathcal{Q}$ be the set of Q-ary modulation symbols, with the mapping rule defined by $\big(\alpha_1^\ell,\ldots,\alpha_q^\ell\big)_{\alpha_i^\ell\in\{0,1\}} \rightarrow s_\ell \in \mathcal{Q}$, where $q = \log_2(Q)$. Then, thanks to (12), the LLRs at the output of SBC (see Fig. 1) can be calculated by a low-complexity procedure as follows

$$\begin{aligned} L_{P,k}^1(i) = &\max_{s_\ell\in\mathcal{Q}|\alpha_i=1}{}^{*}\left(-\frac{|y_k-\mu_k s_\ell|^2}{\sigma_{\xi_k}^2} + \sum_{j=1}^{q}\chi(\alpha_j^\ell)\frac{L_{A,k}^1(j)}{2}\right) \\ &- \max_{s_\ell\in\mathcal{Q}|\alpha_i=0}{}^{*}\left(-\frac{|y_k-\mu_k s_\ell|^2}{\sigma_{\xi_k}^2} + \sum_{j=1}^{q}\chi(\alpha_j^\ell)\frac{L_{A,k}^1(j)}{2}\right), \end{aligned} \tag{13}$$

where $\chi(\alpha) = 2\alpha - 1$ and $\max^*$ denotes Jacobian logarithm, which is defined by

$$\max_i{}^{*}(a_i) = \max^{*}\big(\ldots\max^{*}\big(\max^{*}(a_1,a_2),a_3\big)\ldots,a_i\big), \tag{14}$$

with $\max^*(a_1,a_2) = \max(a_1,a_2) + \ln(1+e^{-|a_1-a_2|})$. On the other hand, the symbol $\tilde{s}_k$ in the k^{th} stream of the IC output is estimated by

$$\begin{aligned} \tilde{s}_k = \mathrm{E}\left[s_k|L_{A,k}^1\right] &= \sum_{s_\ell\in\mathcal{Q}} s_\ell P(s_k = s_\ell|L_{A,k}^1), \\ &= \sum_{s_\ell\in\mathcal{Q}} s_\ell \prod_{i=1}^{q} P(\alpha_i = \alpha_i^\ell|L_{A,k}^1). \end{aligned} \tag{15}$$

The estimated vector $\tilde{\mathbf{s}}$ is then used in the next iteration to find the IC output as shown in (6).

III. Analysis

A. EXIT chart

In this subsection, we would like to illustrate the convergence properties and the advantages of using precoder on the performance of turbo equalization. The EXIT chart, which is proposed by Ten-Brink in [21], [22] and later widely

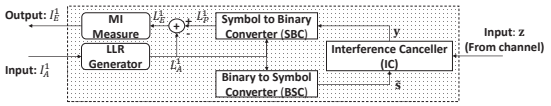

(a) EXIT function of IC.

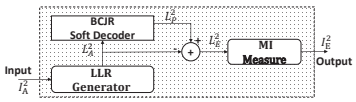

(b) EXIT function of BCJR.

Fig. 5: Block model for the EXIT chart measurement.

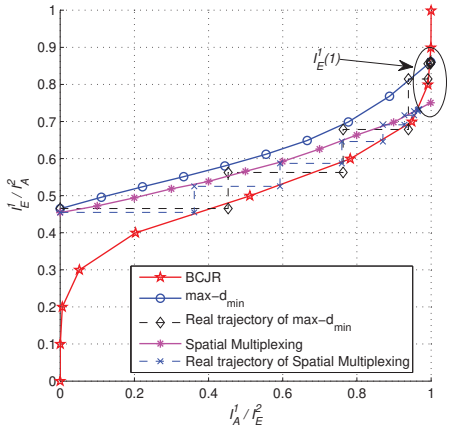

Fig. 6: EXIT chart comparison between max-$d_{\min}$ and Spatial Multiplexing at SNR = 10 dB.

applied in iterative concatenated system analyses [23]–[25], is used to track the evolution of the MI exchanges in the IC detection and FEC decoding process of the iterative system. The LLRs are generated from the MI thanks to the LLR generator block as shown in Fig. 5. The *extrinsic* MI measured at output of SBC is a function of the *a priori* knowledge I_A^1 and the SNR. We define $I_E^1 = T_1\left(I_A^1, \text{SNR}\right)$. Similarly, the *extrinsic* MI at output of BCJR decoder is $I_E^2 = T_2\left(I_A^2\right)$, where I_A^2 stands for its *a priori* knowledge. The mathematical expressions of T_1 and T_2, which were deeply explained in [26], [27] are skipped in this paper. The mutual information is averaged over 100 trials. The signal-to-noise ratio is defined as SNR $= \frac{\sigma_s^2}{\sigma_\eta^2}$. Note that, for the EXIT chart analysis, we normalize $\|\mathbf{H}\|_F^2 = \rho^2 = 1$, *i.e.* the channel energy is included in the SNR and the channel is only characterized by the angle γ.

In Fig. 6, we consider a fixed energy normalized channel $\mathbf{H} = [2\ 1; 1\ 1]/\sqrt{7}$, which was also used in [28], [29], at SNR = 10 dB. The solid line marked by pentagram stands for the EXIT function of the BCJR decoder, which combines with the EXIT function of IC to obtain the EXIT charts of turbo equalization. Two cases namely max-$d_{\min}$ precoder and the spatial multiplexing are considered. The dashed lines show the trajectories. Simulations of the corresponding turbo equalization schemes match with the EXIT chart prediction.

Let us denote $I_E^1(1)$ the *extrinsic* MI at output of SBC at the convergence state, *i.e.* at $I_A^1 = 1$. As shown in Fig. 6, the $I_E^1(1)$ of precoder max-$d_{\min}$ is higher than the spatial multiplexing one. It means that the max-$d_{\min}$ precoded system has a lower

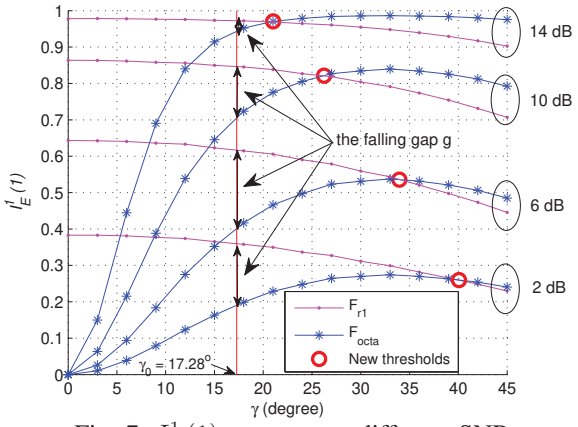

Fig. 7: $I_E^1(1)$ versus γ at different SNR.

error-floor. In addition, the opening of tunnel between the two EXIT functions corresponding to max-$d_{\min}$ is wider, which means that the turbo equalizer with max-$d_{\min}$ converges faster than with the spatial multiplexing. Moreover, the SNR lower-bound, which avoids early crossing of EXIT chart, is lower with the opening of tunnel. These properties are demonstrated by error-rate simulation in Section IV.

B. Convergence state analysis

Recall that the threshold γ_0, which is used to switch between $\mathbf{F}_{r1}$ and $\mathbf{F}_{octa}$ of the precoder max-$d_{\min}$, was selected so as to maximize the $d_{\min}$ of the received constellation points for the uncoded systems. In this subsection, we focus on the convergence state of the turbo equalization to show that the performance corresponding to the max-$d_{\min}$ precoder can be further optimized by selecting a new threshold for each SNR such that the $I_E^1(1)$ is maximized.

Fig. 7 shows the plots in terms of $I_E^1(1)$ of both $\mathbf{F}_{r1}$ and $\mathbf{F}_{octa}$, for all values of γ, at each SNR. Note that $\rho^2 = 1$ in this case. The interest of this figure is threefold. First, it shows that, using the original threshold γ_0, there is a falling gap g between the $I_E^1(1)$ of $\mathbf{F}_{r1}$ and the one of $\mathbf{F}_{octa}$, *i.e.* the $I_E^1(1)$ at the $\gamma > \gamma_0$ is smaller than the counterpart, which reduces the performance. Therefore, we need to select a new threshold γ_{th} (see the bold circles in Fig. 7) that takes into account the turbo equalization assumption. Second, we found that γ_{th} is a function of SNR satisfying $\gamma_{th} > \gamma_0$. Third, we obtain that the falling gap g is very small at the very high SNR, *i.e.* the difference in terms of $I_E^1(1)$ between the original threshold γ_0 and the new one is not significant.

Fig. 8 shows the fitting curve as a function of SNR, which is obtained by plotting the new thresholds defined in Fig. 7 for many different SNRs and fitting the obtained values with the least-squares method [30, Chapter 6]. Similar to the falling gap g, the difference between γ_0 and the new γ_{th} is inversely proportional to the SNR. This is in accordance with the simulation results in next section. The obtained fitting function $\gamma_{th}(x)$ is a cubic polynomial, which reads

$$\gamma_{th}(x) = \alpha_4 + \alpha_3 x + \alpha_2 x^2 + \alpha_1 x^3, \tag{16}$$

where x is SNR in dB, $\alpha_1 = 8.66524 \times 10^{-3}, \alpha_2 = -0.19457, \alpha_3 = -0.50131$ and $\alpha_4 = 42.15576$. The $\gamma_{th}(x)$

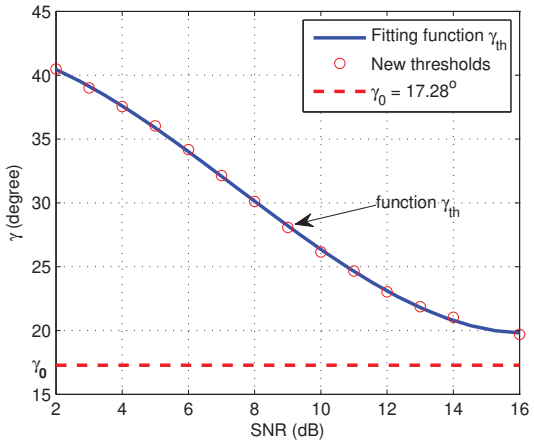

Fig. 8: The new threshold γ_{th} in function of SNR.

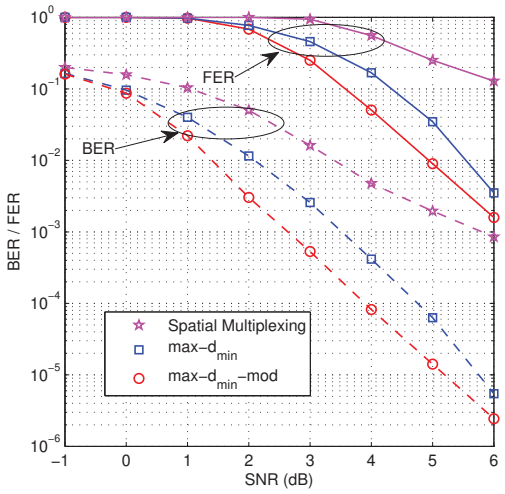

Fig. 9: BER (dashed lines) and FER (solid lines) performance of the precoded turbo equalization in a 2×2 MIMO system.

is measured in degree and the fitting is obtained for $x \in \{2, \ldots, 16\}$. For the region $x > 16$, we fix $\gamma_{th} = 20^o$. The region $x < 2$ is not interesting due to the early crossing in the EXIT chart of the turbo equalization.

In summary, instead of using the static threshold γ_0 to switch between $\mathbf{F}_{r1}$ and $\mathbf{F}_{octa}$ as max-$d_{\min}$ does, we propose the new threshold γ_{th} for each SNR as presented in (16). The new precoder, that uses γ_{th}, is now referred to as max-$d_{\min}$-mod precoder.

IV. Simulation

A randomly generated MIMO channel is considered for the Monte-Carlo simulation, *i.e.* each element of $\mathbf{H}$ is distributed as $\mathrm{H}_{i,j} \sim \mathcal{CN}(0, 1)$. Since, in average, each channel element has unit energy, *i.e* $\mathrm{E}[|\mathrm{H}_{ij}|^2] = 1$ or $\mathrm{E}[||\mathbf{H}||_F^2] = n_T n_R$, we normalize $||\mathbf{H}||_F^2 = \rho^2 = n_T n_R$ to ensure no artificial amplification for each channel realization. Note that this is equivalent to include the channel energy ρ^2 in the SNR, the error-rate performance does not depend on ρ^2. Therefore, we can obtain the system performance for different values of γ by taking the average of the randomly generated channels. The half-rate $(13, 15)_{octal}$-RSC code is used as FEC encoder. The frame length is set to 2000 uncoded bits and interleaved by a random interleaver. Note that, in (13), the approximation $\overset{*}{\max} \approx \max$ yields a similar error-rate performance.

A. 2×2 *MIMO system*

In this subsection, we focus on a MIMO system with $n_T = 2$ transmit and $n_R = 2$ receive antennas (MIMO 2×2) configuration. Fig. 9 shows the bit-error-rate (BER) performance of the turbo equalization when the spatial multiplexing, max-$d_{\min}$ and max-$d_{\min}$-mod precoders are used at the transmitter side. We observe that the MIMO precoder used with turbo equalization significantly improves the system performance. More precisely, the max-$d_{\min}$ precoder achieves a gain of 1.5 dB at BER $= 10^{-2}$ and of 2.5 dB at BER $= 10^{-3}$ compared to the spatial multiplexing. The gain is even larger in the high SNR region, which is in accordance with the analysis in Fig. 6, since the MI at the convergence state, $I_E^1(1)$, of max-$d_{\min}$ is higher than the one of spatial multiplexing.

Moreover, it is shown from Fig. 9 that, by using the proposed threshold γ_{th}, the max-$d_{\min}$-mod precoder respectively achieves a gain of roughly 1 dB and of 0.8 dB at BER $= 10^{-3}$ and BER $= 10^{-4}$ compared to max-$d_{\min}$ precoder. In addition, the performance of max-$d_{\min}$ and max-$d_{\min}$-mod precoder are close to each other at the very high SNR. This confirms the conclusion drawn from Section III-B that, at the very high SNR, γ_{th} is close to γ_0. Similar observations are obtained in terms of frame-error-rate (FER).

Let us pick up an example of using γ_{th} function in Fig. 8 to show the link in terms of SNR between the EXIT chart analysis ($\rho^2 = 1$) and the error-rate simulation ($\rho^2 = n_T n_R$). With $\rho^2 = n_T n_R = 4$, the SNR = 2 dB in Fig. 9 corresponds to the SNR $= 2 + 10\log_{10}(n_T n_R) \simeq 8$ dB in Fig. 8, which gives $\gamma_{th} \simeq 30^o$. The connection holds for other MIMO systems.

B. Comparison with other MIMO systems

In this subsection, we consider another MIMO system with $n_T = 2$ transmit and $n_R = 4$ receive antennas (MIMO 2×4) configuration and compare it with the MIMO 2×2. Fig. 10 shows the BER performance in comparison between the 2×4 and 2×2 MIMO system. We observe that, by increasing the antenna diversity, the 2×4 system performs better than the 2×2 system. However, the performance gain by using the max-$d_{\min}$ and max-$d_{\min}$-mod precoder is less than the gain obtained from 2×2 system. More precisely, the max-$d_{\min}$ precoder achieves a gain of 1.5 dB at BER $= 10^{-4}$ and more than 2 dB at BER $< 10^{-4}$ compared to the spatial multiplexing. In addition, by using the max-$d_{\min}$-mod precoder, the performance is improved by 0.5 dB at BER $= 10^{-4}$ compared to max-$d_{\min}$ precoder. Finally, we can conclude that the improvement of max-$d_{\min}$-mod precoder is more significant for the 2×2 MIMO system.

V. Conclusion

An optimization of the channel angle threshold of max-$d_{\min}$ precoder under the assumption of turbo equalization at the

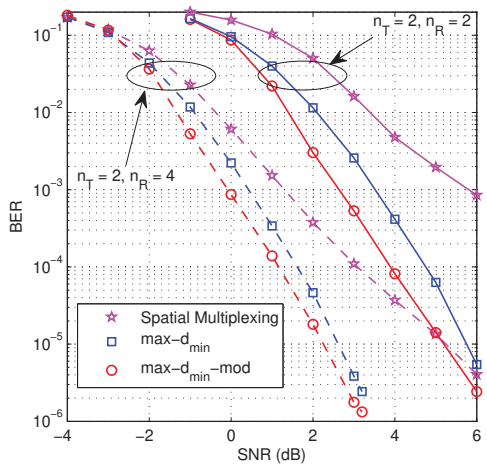

Fig. 10: BER performance of the precoded turbo equalization in comparison between a 2×4 (dashed lines) and the 2×2 (solid lines) MIMO system.

receiver is proposed in this paper. The EXIT chart, which is a good tool to predict the convergence behavior of the iterative receivers, is considered. Thanks to the EXIT chart analysis, we have shown that the *extrinsic* MI at the convergence state, *i.e.* $I_E^1(1)$, corresponding to the $\max$-$d_{\min}$ precoder is higher than with spatial multiplexing. Moreover, the $\max$-$d_{\min}$-mod precoder, which keeps the same structure of $\mathbf{F}_{r1}$ and $\mathbf{F}_{octa}$ but uses the newfound threshold γ_{th}, is proposed in this paper. Simulations show high improvement in terms of error-rate of the MIMO scheme. In addition, there is also a significant gain of $\max$-$d_{\min}$-mod compared to $\max$-$d_{\min}$ precoder. As future work, we propose to optimize the precoder structure assuming turbo equalization at the receiver and taking advantage of the EXIT chart to maximize $I_E^1(1)$.

ACKNOWLEDGMENT

The authors would like to acknowledge Dr. Robert G. Maunder, University of Southampton, UK, for the helpful discussion about EXIT chart analysis.

REFERENCES

[1] C. Berrou and A. Glavieux, "Near optimum error correcting coding and decoding: Turbo-codes," *IEEE Trans. on Commun.*, vol. 44, no. 10, pp. 1261–1271, 1996.

[2] C. Douillard, M. Jézéquel, C. Berrou, D. Electronique, A. Picart, P. Didier, and A. Glavieux, "Iterative correction of intersymbol interference: Turbo-equalization," *European Trans. on Telecommun.*, vol. 6, no. 5, pp. 507–511, 1995.

[3] X. Wang and H. V. Poor, "Iterative (turbo) soft interference cancellation and decoding for coded cdma," *IEEE Trans. Commun.*, vol. 47, no. 7, pp. 1046–1061, 1999.

[4] M. Witzke, S. Baro, F. Schreckenbach, and J. Hagenauer, "Iterative detection of MIMO signals with linear detectors," in *IEEE Asilomar Conf. Signals, Systems and Computers*, vol. 1, 2002, pp. 289–293.

[5] K. Amis, L. Le Josse, and C. Laot, "Efficient frequency-domain MMSE turbo equalization derivation and performance comparison with the time-domain counterpart," in *IEEE Int. Conf. on Wireless and Mobile Commun.*, 2007, pp. 65–65.

[6] K. Amis, G. Sicot, and D. Leroux, "Reduced complexity near-optimal iterative receiver for wimax full-rate space-time code," in *IEEE Int. Symp. on Turbo Codes and Related Topics*, 2008, pp. 102–106.

[7] Q. Li, G. Li, W. Lee, M. Lee, D. Mazzarese, B. Clerckx, and Z. Li, "MIMO techniques in WiMAX and LTE: a feature overview," *IEEE Commun. Mag.*, vol. 48, no. 5, pp. 86–92, 2010.

[8] A. J. Paulraj, D. A. Gore, R. U. Nabar, and H. Bolcskei, "An overview of MIMO communications-a key to gigabit wireless," *Proc. of the IEEE*, vol. 92, no. 2, pp. 198–218, 2004.

[9] V. Tarokh, N. Seshadri, and A. R. Calderbank, "Space-time codes for high data rate wireless communication: Performance criterion and code construction," *IEEE Trans. Info. Theory*, vol. 44, no. 2, pp. 744–765, 1998.

[10] S. Alamouti, "A simple transmit diversity technique for wireless communications," *IEEE J. Sel. Areas Commun.*, vol. 16, no. 8, pp. 1451–1458, 1998.

[11] V. Tarokh, H. Jafarkhani, and A. R. Calderbank, "Space-time block coding for wireless communications: performance results," *IEEE J. Sel. Areas Commun.*, vol. 17, no. 3, pp. 451–460, 1999.

[12] P. Bouvet, M. Hélard, and V. Le Nir, "Low complexity iterative receiver for linear precoded MIMO systems," in *IEEE Symposium on Spread Spectrum Techniques and Applications*, 2004, pp. 17–21.

[13] P. Bouvet, M. Hélard, J. L. Masson, and C. Langlais, "Iterative receiver for linear precoded MIMO systems," in *IEEE ITG-Conference on Source and Channel Coding*, 2006, pp. 1–6.

[14] L. Collin, O. Berder, P. Rostaing, and G. Burel, "Optimal minimum distance-based precoder for MIMO spatial multiplexing systems," *IEEE Trans. on Signal Processing*, vol. 52, no. 3, pp. 617–627, 2004.

[15] P. Rostaing, O. Berder, G. Burel, and L. Collin, "Minimum BER diagonal precoder for MIMO digital transmissions," *Signal Processing*, vol. 82, no. 10, pp. 1477–1480, 2002.

[16] E. Telatar, "Capacity of multi-antenna gaussian channels," *Eur. Trans. Telecommun.*, vol. 10, no. 6, pp. 585–595, 1999.

[17] M. S. Hassan and K. Amis, "On the design of full-rate full-diversity space-time block codes for MIMO systems with a turbo minimum mean square error equaliser at the receiver side," *IET Communications*, vol. 6, no. 18, pp. 3065–3074, 2012.

[18] L. Bahl, J. Cocke, F. Jelinek, and J. Raviv, "Optimal decoding of linear codes for minimizing symbol error rate," *IEEE Trans. on Info. Theory*, pp. 284–287, Mar. 1974.

[19] M. Tuchler, A. C. Singer, and R. Koetter, "Minimum mean squared error equalization using a priori information," *IEEE Trans. Signal Processing*, vol. 50, no. 3, pp. 673–683, 2002.

[20] C. Laot, R. Le Bidan, and D. Leroux, "Low-complexity MMSE turbo equalization: a possible solution for edge," *IEEE Trans. Wireless Commun.*, vol. 4, no. 3, pp. 965–974, 2005.

[21] S. Ten-Brink, J. Speidel, and R.-H. Yan, "Iterative demapping and decoding for multilevel modulation," in *IEEE Global Telecommunications Conference, 1998. GLOBECOM 1998*, vol. 1, 1998, pp. 579–584.

[22] S. Ten-Brink, "Designing iterative decoding schemes with the extrinsic information transfer chart," *AEU Int. J. Electron. Commun.*, vol. 54, no. 6, pp. 389–398, 2000.

[23] ——, "Convergence behavior of iteratively decoded parallel concatenated codes," *IEEE Trans. Commun.*, vol. 49, no. 10, pp. 1727–1737, 2001.

[24] R. G. Maunder, J. Wang, S. X. Ng, L.-L. Yang, and L. Hanzo, "Iteratively decoded irregular variable length coding and trellis coded modulation," in *IEEE Workshop on Signal Processing Systems*, 2007, pp. 222–227.

[25] R. G. Maunder and L. Hanzo, "Iterative decoding convergence and termination of serially concatenated codes," *IEEE Trans. Vehicular Tech.*, vol. 59, no. 1, pp. 216–224, 2010.

[26] M. Tüchler, S. Ten Brink, and J. Hagenauer, "Measures for tracing convergence of iterative decoding algorithms," in *The 4th IEEE/ITG Conf. on Source and Channel Coding*. Citeseer, 2002.

[27] J. Hagenauer, "The exit chart-introduction to extrinsic information transfer in iterative processing," in *Proc. 12th EUSIPCO*, 2004, pp. 1541–1548.

[28] C. Xiao, Y. R. Zheng, and Z. Ding, "Globally optimal linear precoders for finite alphabet signals over complex vector gaussian channels," *IEEE Trans. on Signal Processing*, vol. 59, no. 7, pp. 3301–3314, 2011.

[29] D. P. Palomar and S. Verdú, "Gradient of mutual information in linear vector gaussian channels," *IEEE Trans. on Info. Theory*, vol. 52, no. 1, pp. 141–154, 2006.

[30] W. Gander and J. Hrebicek, *Solving problems in scientific computing using Maple and Matlab®*. Springer Science & Business Media, 2004.